

Cite this: *Soft Matter*, 2014, 10, 8448

## Tuning the surface properties of hydrogel at the nanoscale with focused ion irradiation

 Y. Kim,<sup>a</sup> A. Y. Abuelfilat,<sup>a</sup> S. P. Hoo,<sup>b</sup> A. Al-Abboodi,<sup>b</sup> B. Liu,<sup>a</sup> Tuck Ng,<sup>a</sup> P. Chan<sup>c</sup> and J. Fu<sup>\*a</sup>

With the site-specific machining capability of Focused Ion Beam (FIB) irradiation, we aim to tailor the surface morphology and physical attributes of biocompatible hydrogel at the nano/micro scale particularly for tissue engineering and other biomedical studies. Thin films of Gtn-HPA/CMC-Tyr hydrogels were deposited on a gold-coated substrate and were subjected to irradiation with a kiloelectronvolt (keV) gallium ion beam. The sputtering yield, surface morphology and mechanical property changes were investigated using Scanning Electron Microscopy (SEM), Atomic Force Microscopy (AFM) and Monte Carlo simulations. The sputtering yield of the hydrogel was found to be approximately  $0.47 \mu\text{m}^3 \text{nC}^{-1}$  compared with Monte-Carlo simulation results of  $0.09 \mu\text{m}^3 \text{nC}^{-1}$ . Compared to the surface roughness of the pristine hydrogel at approximately 2 nm, the average surface roughness significantly increased with the increase of ion fluence with measurements extended to 20 nm at  $100 \text{ pC } \mu\text{m}^{-2}$ . Highly packed submicron porous patterns were also revealed with AFM, while significantly decreased pore sizes and increased porosity were found with ion irradiation at oblique incidence. The Young's modulus of irradiated hydrogel determined using AFM force spectroscopy was revealed to be dependent on ion fluence. Compared to the original Young's modulus value of 20 MPa, irradiation elevated the value to 250 MPa and 350 MPa at  $1 \text{ pC } \mu\text{m}^{-2}$  and  $100 \text{ pC } \mu\text{m}^{-2}$ , respectively. Cell culture studies confirmed that the irradiated hydrogel samples were biocompatible, and the generated nanoscale patterns remained stable under physiological conditions.

Received 15th May 2014  
Accepted 18th August 2014

DOI: 10.1039/c4sm01061b

www.rsc.org/softmatter

### 1. Introduction

Hydrogels are crosslinked networks composed of either natural or synthetic polymers, and the hydrophilic properties of hydrogels make them great materials for bioengineering.<sup>1,2</sup> It is well known that the shapes and physicochemical properties of hydrogels have a strong influence on cell growth and migration, and various approaches have been developed to tune these properties for improved cell growth and biocompatibility. For example, porosity and pore size could be altered through additional porogens, freeze-drying, photopatterning, foam generation, *etc.*,<sup>3-7</sup> while the elastic modulus is a function of component concentrations.<sup>8,9</sup> It has recently been suggested that, in addition to physical and chemical properties, topographic properties at the micro and nanoscale play a critical role in cellular interaction with its surrounding environment.<sup>10-13</sup> For tissue engineering applications, it is now also advantageous to create nanoscale features on the surface with properties

similar to those in the extracellular matrix in order to control cellular behaviour and enhance cell growth, adhesion and proliferation.<sup>10,11,13-15</sup>

Previous studies on shape control of surface nanotopology were typically based on soft lithography<sup>16</sup> or the intrinsic elastic property,<sup>16,17</sup> predominantly on polydimethylsiloxane (PDMS); however, there are only limited reports on altering the surface topology of hydrogels at the micro and nanoscale, possibly due to the technical difficulties involved in fabricating micro/nanoscale structures on soft materials, or a limited knowledge of the fundamental mechanisms involved. Recent reports showed that ion beam irradiation was capable of forming nanoscale wrinkle features on polymer surfaces.<sup>18-24</sup> Typically equipped with a gallium ion ( $\text{Ga}^+$ ) or helium ion ( $\text{He}^+$ ) source, a modern Focused Ion Beam (FIB) instrument allows the accelerated ions to perform site-specific milling with electrostatic lenses.<sup>25-27</sup> In conjunction with scanning electron microscopy (SEM), micro- and nano-machining with resolution in nanometers down to single digits can be done while imaging and analysing at the same time. FIB/SEM has been successfully applied for imaging applications such as three-dimensional hydrogels,<sup>4</sup> cell-material interfaces and even single cells.<sup>28-30</sup> However, the capability of site-specific FIB milling is not fully utilized for biomaterial applications.

<sup>a</sup>Department of Mechanical and Aerospace Engineering, Monash University, Clayton, VIC, 3800, Australia. E-mail: jing.fu@monash.edu

<sup>b</sup>Department of Chemical Engineering, Monash University, Clayton, VIC, 3800, Australia

<sup>c</sup>School of Applied Science, RMIT University, 3000, Australia

An example of a periodic pattern of micron size dots presented in Fig. 1a was designed and preliminarily patterned on a hydrogel surface within minutes, without the use of chemicals or sophisticated masks. This provided a quick method for fabricating nano/micro scale features on hydrogel, and the final pattern was visible by optical microscopy with clearly defined geometry (Fig. 1b). Under SEM, however, some morphological artefacts on the surface could be observed, and inconsistent geometries such as the milling depth were also present due to a lack of information (Fig. 1c). As such, the primary aim of the present research is to provide an in-depth investigation on the surface topology and physical properties of hydrogel at the nano/micro scale by utilizing FIB to achieve designed patterns of high precision. The engineering issues including yield and angular effects were investigated through both Monte Carlo simulations and experimental studies. Other questions such as surface roughness and modulus of the hydrogel were measured by Atomic Force Microscopy (AFM) prior to and after ion irradiation. Based on these results, patterns on hydrogel with tailored surface topology and physical attributes could be precisely achieved by setting the beam parameters, *e.g.* acceleration voltage, ion fluence and incident angle. The compatibility and stability of the patterned hydrogels were also tested in cell culture to demonstrate the applicability of this patterning method for bioapplications.

## 2. Materials and methods

### Sample preparation

Carboxymethylcellulose–tyramine (CMC–Tyr) and gelatin–hydroxyphenylpropionic acid (Gtn–HPA) were synthesized according to ref. 4. CMC–Tyr and Gtn–HPA conjugates were each dissolved in a phosphate buffer saline (PBS) solution at a concentration of 5%. A hydrogel precursor solution was prepared by mixing Gtn–HPA and CMC–Tyr in an 80 : 20 weight ratio, respectively. This precursor went through a vigorous vortex for a few minutes. Horseradish peroxide (HRP) and diluted H<sub>2</sub>O<sub>2</sub> were then added to the precursor as cross-linking reagents; each reagent was pre-diluted with PBS solution. A final concentration of 15.5 units per L of HRP and  $49.8 \times 10^{-6}$  M of H<sub>2</sub>O<sub>2</sub> was used in this research. This precursor was then

vigorously vortexed for a few minutes. The pH level of the hydrogel PBS solution before and after cross-linking was measured using a pH meter (Thermo Fisher Scientific, Scoresby, VIC Australia). For the PBS solution, the pH level was measured to be 7.51 and the pH level of the hydrogel before and after cross-linking was 7.35 and 7.41, respectively.

An aliquot of 100  $\mu$ L of the precursor was deposited on a gold plated cover glass and any air bubbles were removed by gently stirring with the tip of a micropipette. In order to achieve a thin, uniform layer of hydrogel, spin coating was performed in three stages. In the first stage, spin coating was carried out at 500 rpm for 10 seconds, followed by 3000 rpm for 40 seconds. Finally, another 500 rpm for 10 seconds of spin coating provided a thin uniform layer of mixture with a thickness of approximately 1  $\mu$ m. The precursor was then allowed to cross-link to form the hydrogel.

### Focused Ion Beam (FIB) irradiation

FIB milling was performed on a FIB/SEM system (FEI Helios NanoLab 600) equipped with a gallium liquid metal ion source (LMIS). Thin films of hydrogel samples were first transferred to the system chamber until high vacuum status was reached. The ion current used in the experiment ranged from 0.92 pA to 0.97 nA. Without additional notes, default overlapping and dwell time were 0% and 3  $\mu$ s, respectively. The ion fluence of Ga<sup>+</sup> ranging from 0.05 pC  $\mu$ m<sup>-2</sup> to 600 pC  $\mu$ m<sup>-2</sup> was regulated to irradiate a  $10 \times 10 \mu$ m square region. The default incident angle was kept at 0° (normal incidence), and to study the effect of the incident angle, the stage was tilted from 0° to 62°. SEM images were typically acquired with a secondary electron detector with a 5 keV acceleration voltage and 86 pA current.

### Atomic force microscopy (AFM)

Surface properties were examined using an AFM instrument (Dimension Icon, Bruker Corporation, Santa Barbara, CA, US) in a cleanroom environment. For measuring the surface topology, cantilevers with a 70 kHz resonance frequency and 0.4 N m<sup>-1</sup> spring constant were used. By default,  $20 \times 20 \mu$ m regions were scanned to obtain reliable statistics. The sputtering yield of the hydrogel was calculated by examining the volume removed by the ion beam irradiation and ion fluence applied. Surface roughness and the characteristics of regular patterns were calculated using the software package NanoScope Analysis 1.4 (Bruker Corporation, Santa Barbara, CA, US). For the force measurements and modulus calculations, a cantilever with a 0.06 N m<sup>-1</sup> spring constant was used to accommodate the low modulus of the hydrogel sample with a JPK NanoWizard2 AFM (JPK Instruments AG, Berlin, Germany) under ambient conditions. Calibration of the cantilever was conducted prior to the force mapping using a mica sheet, measuring the sensitivity and spring constant of the cantilever. Force mapping of the sample of  $5 \times 5 \mu$ m regions were done at  $16 \times 16$  resolution. Analysis was carried on using JPKSPM Data Processing software (JPK Instruments AG, Berlin, Germany) which allows batch processing.

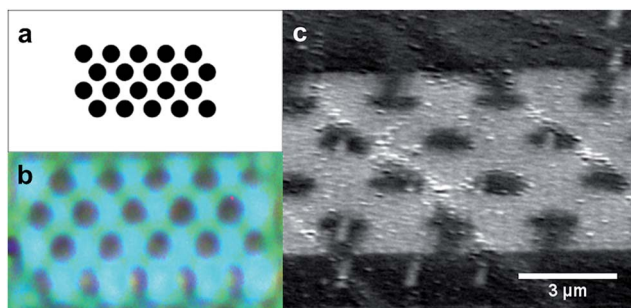


Fig. 1 Site-specific patterning on hydrogel with Focused Ion Beam (FIB) irradiation. (a) Designed pattern and (b) optical image of the corresponding 1  $\mu$ m diameter dots after patterning. (c) Low current SEM image showing the detailed dots during ion milling.

### SRIM Monte-Carlo simulation

A Monte-Carlo simulation of the sputtering process of hydrogel was performed with the software package SRIM (The Stopping and Range of Ions in Matter) version 2013.<sup>31</sup> The hydrogel was set up as a new compound consisting of carbon, hydrogen and oxygen with an atomic stoichiometry of 8 : 8 : 1, respectively. The density of the hydrogel was obtained by measuring the bulk weight and volume, and the average value  $1.655 \text{ g cm}^{-3}$  obtained was input for all of the simulations. At least 5000 ions were simulated in each run, and parameters including the angle of incident and ion energy were varied based on the parameters used in the experiments.

### Cell culture of COS-7 cells and cytotoxicity tests

African green monkey kidney cells (COS-7 cells) were grown and maintained in Dulbecco's Modified Eagle Medium (DMEM) supplemented with 10% fetal bovine serum (FBS), 2 mM L-glutamine, and 50 units per mL penicillin-streptomycin (P-S) at 37 °C in a 5% humidified carbon dioxide incubator. The patterned and unpatterned hydrogel samples and the tissue culture plate were sterilized under UV for 3 h before cell seeding. Cell seeding was conducted at a density of  $3 \times 10^4$  cells per sample, and in each sample, the diameter of the hydrogel thin film was approximately 1 cm. The plate was incubated at 37 °C in a humidified 5% CO<sub>2</sub> incubator for 3 h for cell attachment to take place, and then 3 mL of fresh culture medium was added and the cells were allowed to further cultivate on the hydrogel. Visualization of the cells on the patterned hydrogel was executed using an inverted optical microscope at different time points. The viability of cells after immobilization in the hydrogel was examined using a live/dead viability assay kit, and pristine hydrogels without patterning were used as a control. The hydrogels were incubated in 5  $\mu\text{M}$  calcein acetoxymethyl ester solution (Life Technologies, Australia) for half an hour, followed by 1.5  $\mu\text{M}$  propidium iodide (Life Technologies, Australia) for 5 min in DMEM at 37 °C. Images of live (green) cells were then acquired on day 5 by using an inverted laser confocal fluorescence microscope (Nikon A1 Rsi MP, Australia). For SEM imaging, the samples were then kept in the  $-20 \text{ }^\circ\text{C}$  freezer followed by lyophilization in a freeze-dryer (HETO PowerDry PL6000, Thermo Scientific, Australia) for 24 h.

## 3. Results and discussion

### Milling yield of hydrogel by keV ion beam

The sputtering yield of the hydrogel with ion beam irradiation was measured by the volume loss method and compared with the results from Monte Carlo simulations based on SRIM. Ion fluence applied for determining the yield ranged from 0.05 pC  $\mu\text{m}^{-2}$  to 600 pC  $\mu\text{m}^{-2}$  to obtain an adequate amount of data points prior to significant redeposition, and the sputtering rate was represented as the volume ( $\mu\text{m}^3$ ) removed per ion dose (nC) measured by AFM. The milling was performed on a typical hydrogel surface area of  $10 \times 10 \mu\text{m}$ , and the total volume of material removed was calculated and plotted in Fig. 2a. The sputtering rate of the hydrogel by 30 keV Ga<sup>+</sup>, estimated by the

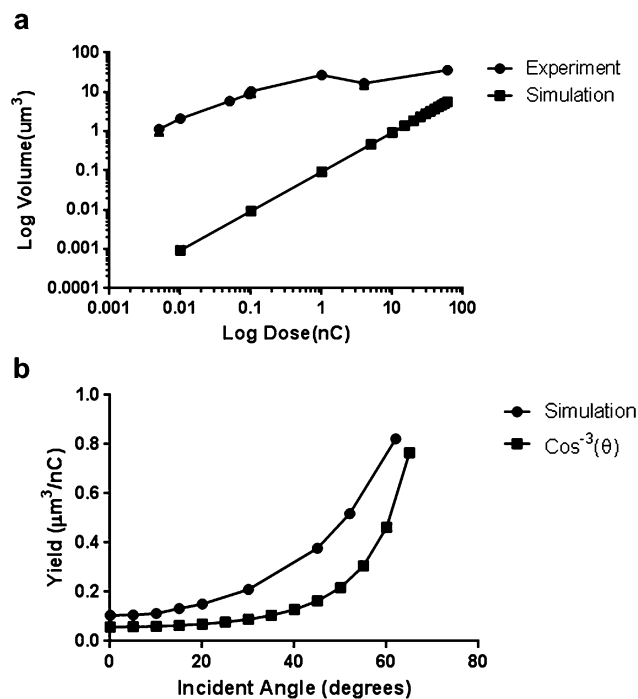


Fig. 2 Investigation of sputtering of hydrogel (Ga<sup>+</sup>, 30 keV) with (a) comparison of sputtering yield based on both experimental data and Monte-Carlo simulations and (b) simulated angular effects on sputtering yield.

gradient of the plotted curve, is  $0.47 \mu\text{m}^3 \text{ nC}^{-1}$ , while the results of MC simulations with SRIM gave a gradient of  $0.09 \mu\text{m}^3 \text{ nC}^{-1}$ ; both are plotted in Fig. 2a for comparison.

The difference between experimental and simulation results could be due to a few reasons. As MC simulation has certain limitations, *e.g.* binding energy of atoms or segregation of elements at the surface is not clearly defined for hydrogel, some estimates were supplemented during the setup phase based on previous reports and data.<sup>21,22</sup> The surfaces of the irradiated hydrogel were roughened as discussed in later sections and contained porous features which may affect the measurements. Some additional effects such as charging during the irradiation of insulated hydrogel as well as redeposition may also have contributed to the variations in simulation.<sup>21,22,32,33</sup> The experimentally determined yield of this study ( $0.47 \mu\text{m}^3 \text{ nC}^{-1}$ ), however, is close to the reported yield of polymethyl methacrylate (PMMA) with the same ion energy,<sup>34</sup> and will provide a reference value for future tasks.

The effect of the beam incident angle (angular effects) on the yield was also investigated. As a rule of thumb, an inverse cosine rule was typically applied, in which the yield increases by  $1/\cos^n(\varphi)$ , where  $\varphi$  is the incident angle measured from the normal of the surface. The simulation result reasonably follows the trend with  $n \approx 3$ , consistent with published results in the literature.<sup>22,35,36</sup> An incident angle larger than  $62^\circ$  could not be directly measured due to the restrictions of the current instrument, and thus was not examined in this study. The yield of hydrogel with ions of different acceleration voltage in the keV range was also simulated with SRIM. The results suggested that

the sputtering yield gradually increased and reached its peak point close to 30 keV. With the acceleration voltage approaching 60 keV, the yield of hydrogel started to decrease. This result also agrees with the trends found in previous reports for various materials.<sup>35,37</sup>

### Surface morphology of irradiated hydrogel

The surface roughness of the hydrogel surface prior to and after irradiation was investigated with AFM, with ion fluence ranging from  $0.05 \text{ pC } \mu\text{m}^{-2}$  to  $100 \text{ pC } \mu\text{m}^{-2}$ . Two examples of ion fluence at  $0.1 \text{ pC } \mu\text{m}^{-2}$  and  $100 \text{ pC } \mu\text{m}^{-2}$  were presented in Fig. 3a and b, respectively. For each obtained image, measurements were performed at multiple locations in both pristine and irradiated regions. At an ion fluence of  $0.1 \text{ pC } \mu\text{m}^{-2}$ , no significant morphological change was observed, and even the original swelling islands on the pristine hydrogel remained unchanged after the irradiation (Fig. 3a). In Fig. 3b, a dramatic porous pattern was introduced on the bottom of the milled cavity after significantly extended irradiation ( $100 \text{ pC } \mu\text{m}^{-2}$ ) compared to the smoother pristine surface. Detailed measurements of the surface roughness are presented in Fig. 3c including side-by-side comparisons with regard to ion irradiation. It is evident that surface roughness was at least doubled after irradiation; however, the average values remained below 10 nm at initial ion fluences. A surge occurred at an ion fluence of  $1 \text{ pC } \mu\text{m}^{-2}$ , and the average surface roughness was elevated to

20 nm at an ion fluence of  $100 \text{ pC } \mu\text{m}^{-2}$ . This result suggests that nanoscale roughening occurs after initial radiation, while after achieving a certain threshold, an erosion-type morphology becomes the dominant appearance on the hydrogel surface.

Previous reports showed directional patterns on polymers,<sup>18,35,38–41</sup> such as oriented ripples, wrinkles, *etc.*, which are mainly induced by the interplay of sputtering erosion and surface relaxation mechanisms, *e.g.* surface expansion which is perpendicular to the direction of the ion beam.<sup>39</sup> In addition to surface roughness, these unique patterns and the distributions are also interesting phenomena and were the subjects of investigations with different ion irradiation parameters in this study. Fig. 4a and b present selected AFM images after FIB irradiation at  $0^\circ$  incident angles (normal) on hydrogel. The incident angle was raised to  $50^\circ$  and  $60^\circ$ , with the results presented in Fig. 4c and d, respectively. A 2D profile of the AFM measurements is presented in Fig. 4g to demonstrate the typical cross-section. Overall, porous structures were observed across all of the irradiated samples, with average diameters in the order of several hundreds of nanometers. Contrary to previous reports, no significant orientation was observed in the patterns generated on the hydrogel surface in this study regardless of the ion fluence or incident angle. This may be due to the fact that synthetic hydrogel possesses more heterogeneous structures compared to single-component polymers, and the sputtering yield was varied across the surface to promote the formation of porous structures. Although it is feasible for hydrogel to have a controlled microscale porous morphology for scaffolding,<sup>4</sup> the proposed ion irradiation approach provides unique controllable submicron pores which are challenging for other approaches.

The patterns measured by AFM were further analysed to obtain details of the submicron pores. By converting the original AFM data to binary images as shown in Fig. 4e and f, porosity, as defined by the percentage of void to overall area, could then be quantified. The measured pore size and porosity at varied ion fluence and incident angles were summarized in Fig. 5a–d. The results showed that the size of the porous patterns was not significantly changed with the increase of ion fluence, and the average pore size and porosity are approximately 600 nm and 0.45 respectively (Fig. 5a and c). This also suggests that pore formation requires limited ion fluence even at  $1 \text{ pC } \mu\text{m}^{-2}$ , and then with the increase in ion fluence, the hydrogel surface underwent uniform erosion with similar porous structures. In comparison, results based on a higher incident angle (50 to 60 degree) showed similar porous structures (Fig. 4c and d) but with significantly smaller pore size and higher porosity (Fig. 5b and d). It is common practice for ion sputtering at oblique incidence to introduce different morphology for inorganic materials.<sup>42</sup> For the current study, the average implantation depth of the incident gallium ion was reduced at higher incident angles, and the overall transferred kinetic energy is in closer proximity to the top surface layer. This allowed sputtering at the top layer to be more effective compared to other dynamic surface mechanisms, and thus resulted in pores of higher density.

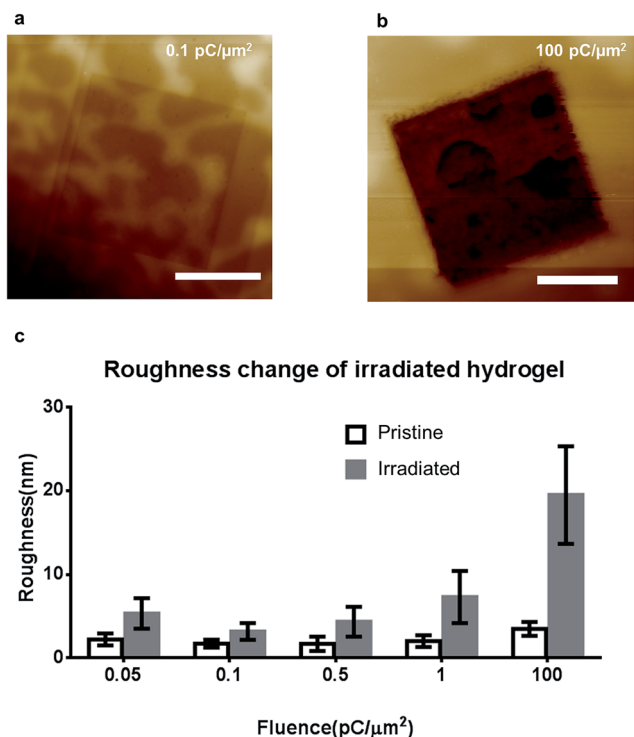


Fig. 3 AFM images (top view) of surface morphology after ion milling ( $\text{Ga}^+$ , 30 keV) with an ion fluence of (a)  $0.1 \text{ pC } \mu\text{m}^{-2}$  and (b)  $100 \text{ pC } \mu\text{m}^{-2}$ . (c) The corresponding numerical values of surface roughness of pristine hydrogel and after ion irradiation with increasing ion fluence (scale bar:  $5 \mu\text{m}$ ).

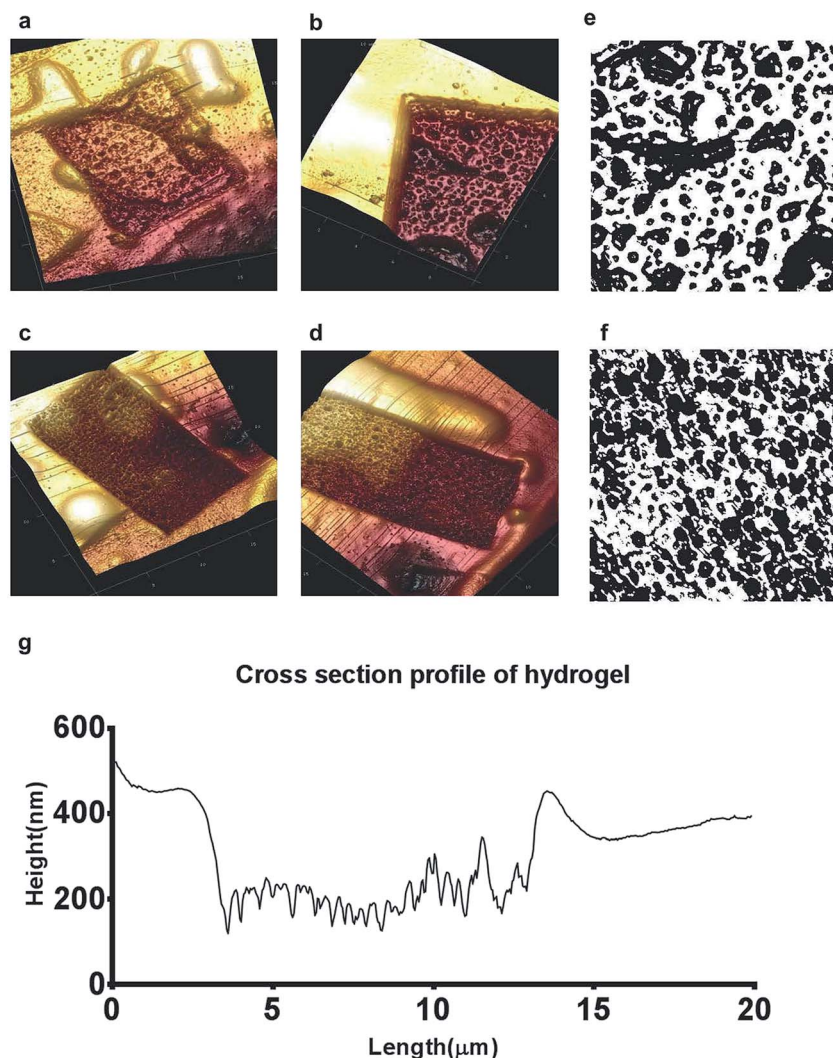


Fig. 4 3D AFM images of the porous patterns after ion irradiation ( $\text{Ga}^+$ , 30 keV) with ion fluence from (a)  $1 \text{ pC } \mu\text{m}^{-2}$ ,  $0^\circ$  incident angle to (b)  $100 \text{ pC } \mu\text{m}^{-2}$ ,  $0^\circ$  incident angle. Porosity increases with the increase of incident angle from (c)  $100 \text{ pC } \mu\text{m}^{-2}$ ,  $52^\circ$  incident angle to (d)  $100 \text{ pC } \mu\text{m}^{-2}$ ,  $62^\circ$  incident angle. The corresponding converted binary images for porosity measurements after irradiation at incident angle (e)  $0^\circ$  and (f)  $62^\circ$ . (g) A cross-section profile of hydrogel after irradiation based on AFM.

### Modulus of irradiated hydrogel

Mechanical elasticity has been widely accepted as a controllable factor for cell growth and differentiation.<sup>9,43</sup> Though it is feasible to tune the elasticity of polymers including hydrogel in bulk forms by varying the concentrations,<sup>8</sup> controlled elasticity modification, particularly at the submicron scale, has never been established. Previous studies<sup>39,44</sup> showed a significantly higher modulus of PDMS after keV ion irradiation, and in the present study, we also aim to investigate the modulus through FIB irradiation *in situ*. The results measured by AFM force spectroscopy are presented in Fig. 6 with ion fluence from  $1 \text{ pC } \mu\text{m}^{-2}$  to  $100 \text{ pC } \mu\text{m}^{-2}$ . Compared to pristine hydrogel, the average modulus was significantly elevated with the increase in ion fluence, from less than 20 MPa for pristine hydrogel to 250 MPa at an ion fluence of  $1 \text{ pC } \mu\text{m}^{-2}$  and 350 MPa at an ion fluence of  $100 \text{ pC } \mu\text{m}^{-2}$ . All the AFM modulus measurements were performed under ambient conditions,

and although preferred, measuring the modulus of hydrogel in liquid medium remains a challenge, as it is well known that hydrogel response in water is varied. Also, in order to accommodate the estimated modulus range of hydrated hydrogel, soft cantilevers with a spring constant of  $0.03 \text{ N m}^{-1}$  were initially used in a few attempts, and cantilevers were likely broken at the air-liquid interface, possibly due to surface tension at the air-liquid interface. The fittings based on a few successful measurements suggested that the modulus of hydrated hydrogel is in the range of 100 kPa to 1 MPa, consistent with the reported hydration induced effects.<sup>45,46</sup> The increased water content in the hydrogel may have resulted in a larger probe-surface contact area, and the actual hydration-modulus relationship after ion irradiation will be an interesting topic for future study.

It is interesting to note that the site-specific modulus tuning of post-crosslinking hydrogel accomplished in this study has

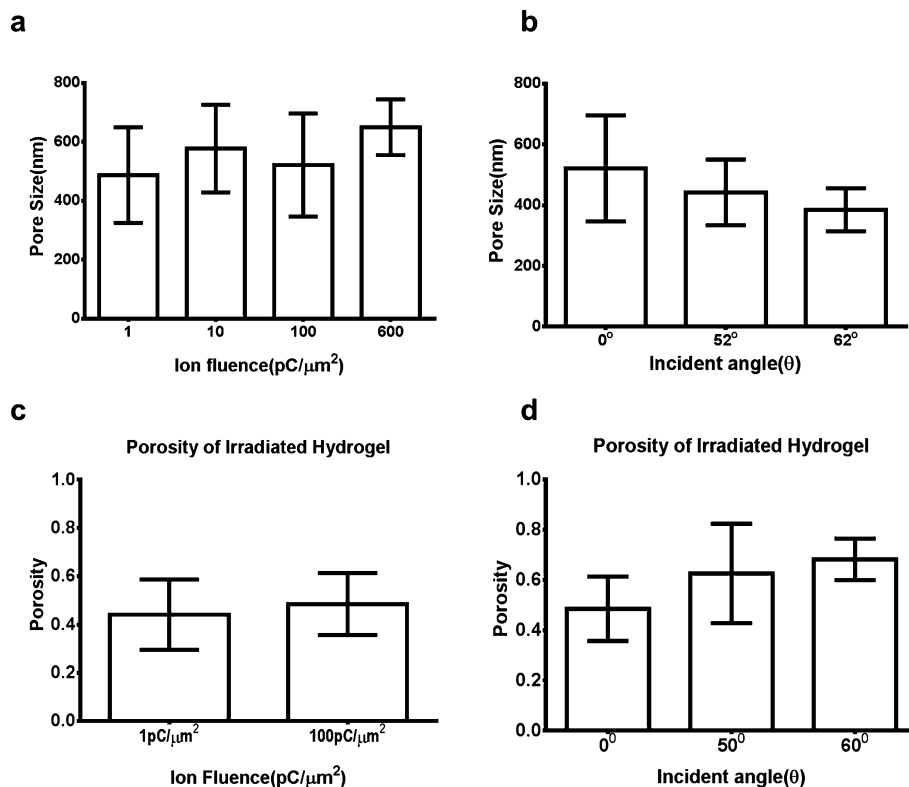


Fig. 5 Numerical values of pore size on hydrogel after ion irradiation ( $\text{Ga}^+$ , 30 keV) measured by AFM with (a) ion fluences ranging from  $1 \text{ pC } \mu\text{m}^{-2}$  to  $600 \text{ pC } \mu\text{m}^{-2}$  and (b) incident angles ranging from  $0^\circ$  to  $62^\circ$ . Data for porosity after irradiation at varied ion fluences and incident angles are presented in (c) and (d).

not been feasible with other existing approaches. Although focused electron beam irradiation was deployed for localized crosslinking of hydrogel,<sup>47,48</sup> the fabricated features were attached to a substrate such as silicon and was not applicable for tissue engineering. A swelling effect of the electron patterned hydrogel was reported, but so far no details on modulus have been provided. In the current study, nuclear

stopping of the gallium ions is expected to be dominant in conjunction with the MC simulation results, and that causes substantial nuclear displacements and scission of bonds in the target hydrogel. A transition from one-dimensional chains into a three-dimensional matrix may provide an explanation for the elevated Young's modulus,<sup>49,50</sup> although a more conclusive study is needed in the future.

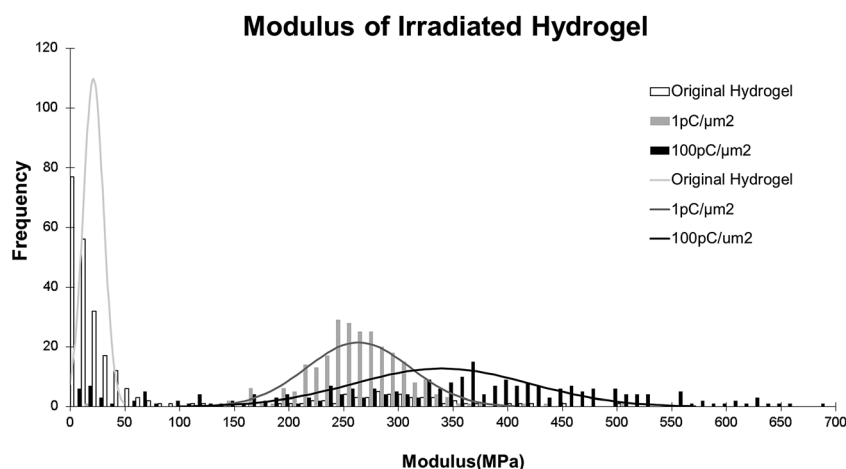


Fig. 6 Young's modulus of hydrogel prior to and after the irradiation ( $\text{Ga}^+$ , 30 keV) with ion fluence from  $1 \text{ pC } \mu\text{m}^{-2}$  to  $100 \text{ pC } \mu\text{m}^{-2}$ . Solid curves represent the fitted normal distributions of the fitted histograms.

## Results of cell culture on patterned hydrogel

To assess the stability of the generated patterns, ion irradiated samples were kept in a physiological environment for 48 h, *i.e.* with the same culture medium and temperature but without seeding cells. After dehydration, the samples were finally investigated with both optical and SEM imaging (Fig. 7a and b), and the original FIB milled patterns were clearly present without noticeable changes. This suggests that the FIB milled patterns are stable in a cell culture environment, at least prior to the controlled dissolution of hydrogel. Although increased

roughness after ion irradiation resulted in a larger contact surface area, hardening of the top layer as shown by the increased modulus may provide an additional barrier against physical and chemical modifications of the patterns.

To demonstrate the biocompatibility of FIB patterning on hydrogel, cell culture experiments were performed on the irradiated samples. Optical images recorded right after seeding and at 44 h after seeding are presented in Fig. 7c–f. For both irradiated and non-irradiated samples, the COS-7 cells reached confluence, and displayed typical spread out morphology. The same morphology was observed in the 10  $\mu\text{m}$  ion irradiated square regions (Fig. 7d) compared to the cells grown on the irradiated hydrogel surface. In addition, confocal microscopy was performed to provide higher magnification investigations, with results presented in Fig. 7g and h. It is clear that, for both irradiated and non-irradiated samples, COS-7 cells were firmly adhered to hydrogel, a scenario consistent with this type of hydrogel in the literature.<sup>4</sup> For the cells grown on the rectangle patterned regions as shown in Fig. 7h, no measurable difference in morphology was found. The viability of these cells was confirmed by the consistent green fluorescent color, without the presence of any dead cells. These results confirmed that gallium ion beam irradiation has negligible effects on cell growth, although gallium is generally considered as toxic.<sup>51,52</sup> From SRIM results, the majority of the incident gallium will eventually be implanted into the target hydrogel, and the free gallium ions, which are a possible source of the toxicity, are expected to be minimal on the hydrogel surface. It can also be inferred that patterns generated by other commercially available FIB sources based on noble gases such as helium, neon, *etc.* will likely be biocompatible, although additional studies to confirm it would be preferable. The results of both experiments presented above prove the stability and compatibility of these nano/micro scale patterns on hydrogel, and pave the way towards various bioapplications.

## 4. Conclusion

In conclusion, Focused Ion Beam milling was performed on the thin films of hydrogel to tune various surface properties including surface morphology and modulus, characterized by electron microscopy and AFM. The sputtering yield of hydrogel by a keV gallium ion beam was examined experimentally and compared to results obtained from Monte-Carlo simulations. It was revealed that the surface roughness was doubled after low dose irradiation, and a significant increase in the Young's modulus was also confirmed. During irradiation, unique nanoscale porous features in regular formation were also observed, and the pore parameters were found to be dependent on ion incident angles. Cell culture experiments confirmed the biocompatibility and stability of the patterns generated based on FIB with gallium sources. Given the *in situ* high precision capability and sufficient yield compared to laser and electron beam based approaches, we expect that the proposed approach will provide tunable submicron features on hydrogel which are unique for future research in tissue engineering and biosensing.

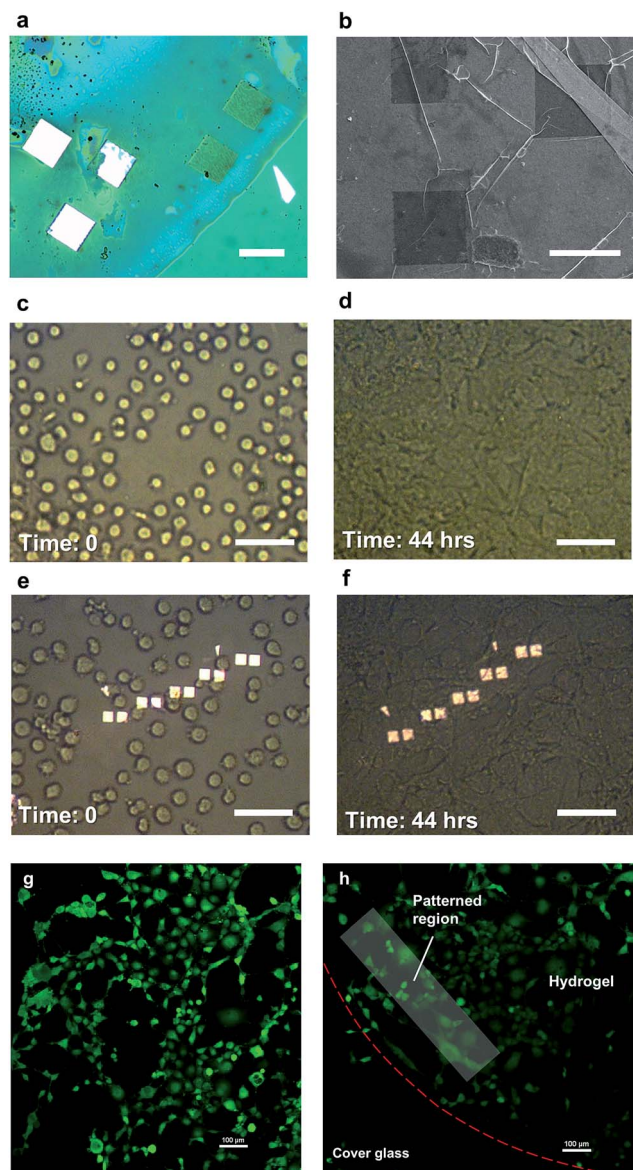


Fig. 7 Without cell seeding: (a) optical image of ion beam induced patterns, compared with (b) the same patterns kept in a physiological environment for 48 h (SEM image). Optical images of cells on non-irradiated hydrogels (c) at 0 h, and (d) at 44 h after cell seeding. Optical images of cells on irradiated hydrogel (e) at 0 h, and (f) at 44 h after cell seeding. Confocal images of cell morphology on (g) the control hydrogel sample, and (h) the patterned hydrogel. (Scale bar: 10  $\mu\text{m}$  in a and b, 50  $\mu\text{m}$  in c–f.)

## Acknowledgements

Funding for this research was partly provided through Australia Research Council Discovery Project Grant (DP120102570 and DP120100583) and Seed Fund of Monash Engineering. This work was performed in part at the Melbourne Centre for Nanofabrication (MCN) in the Victorian Node of the Australian National Fabrication Facility (ANFF). The author would like to thank the staff from MCN for various support and training.

## References

- 1 J. Kopeček, *Biomaterials*, 2007, **28**, 5185–5192.
- 2 A. C. Jen, M. C. Wake and A. G. Mikos, *Biotechnol. Bioeng.*, 1996, **50**, 357–364.
- 3 Q. Liu, E. L. Hedberg, Z. Liu, R. Bahulekar, R. K. Meszlenyi and A. G. Mikos, *Biomaterials*, 2000, **21**, 2163–2169.
- 4 A. Al-Abboodi, J. Fu, P. M. Doran, T. T. Tan and P. P. Chan, *Adv. Healthcare Mater.*, 2013, **3**, 725–736.
- 5 S. J. Bryant, J. L. Cuy, K. D. Hauch and B. D. Ratner, *Biomaterials*, 2007, **28**, 2978–2986.
- 6 S. P. Hoo, Q. L. Loh, Z. Yue, J. Fu, T. T. Y. Tan, C. Choong and P. P. Y. Chan, *J. Mater. Chem. B*, 2013, **1**, 3107–3117.
- 7 J.-y. Lin, W.-j. Lin, W.-h. Hong, W.-c. Hung, S. H. Nowotarski, S. M. Gouveia, I. Cristo and K.-h. Lin, *Soft Matter*, 2011, **7**, 10010–10016.
- 8 J. R. Tse and A. J. Engler, *Curr Protoc Cell Biol.*, 2010, 10.16.11–10.16.16.
- 9 A. J. Engler, S. Sen, H. L. Sweeney and D. E. Discher, *Cell*, 2006, **126**, 677–689.
- 10 F. Boccafosci, M. Rasponi, C. Mosca, E. Bocchi and S. Vesentini, *Adv. Mater.*, 2012, **409**, 109–110.
- 11 Z. Pan, C. Yan, R. Peng, Y. Zhao, Y. He and J. Ding, *Biomaterials*, 2012, **33**, 1730–1735.
- 12 M. M. Stevens and J. H. George, *Science*, 2005, **310**, 1135–1138.
- 13 W. Chen, L. G. Villa-Diaz, Y. Sun, S. Weng, J. K. Kim, R. H. W. Lam, L. Han, R. Fan, P. H. Krebsbach and J. Fu, *ACS Nano*, 2012, **6**, 4094–4103.
- 14 L. Csaderova, E. Martinez, K. Seunarine, N. Gadegaard, C. D. W. Wilkinson and M. O. Riehle, *Small*, 2010, **6**, 2755–2761.
- 15 E. K. F. Yim, E. M. Darling, K. Kulangara, F. Guilak and K. W. Leong, *Biomaterials*, 2010, **31**, 1299–1306.
- 16 P. Kim, W. E. Adorno-Martinez, M. Khan and J. Aizenberg, *Nat. Protoc.*, 2012, **7**, 311–327.
- 17 Y. Zhang, E. A. Matsumoto, A. Peter, P.-C. Lin, R. D. Kamien and S. Yang, *Nano Lett.*, 2008, **8**, 1192–1196.
- 18 M.-W. Moon, S. H. Lee, J.-Y. Sun, K. H. Oh, A. Vaziri and J. W. Hutchinson, *Scr. Mater.*, 2007, **57**, 747–750.
- 19 T. Kaito, in *Introduction to Focused Ion Beams*, ed. L. Giannuzzi and F. Stevie, Springer, US, 2005, ch. 4, pp. 73–86.
- 20 K. M. Lee, A. Neogi, J. M. Perez and T. Y. Choi, *Nanotechnology*, 2010, **21**, 205303.
- 21 J. J. L. Mulders, D. A. M. de Winter and W. J. H. C. P. Duinkerken, *Microelectron. Eng.*, 2007, **84**, 1540–1543.
- 22 H. Ostadi, K. Jiang and P. D. Prewett, *Microelectron. Eng.*, 2009, **86**, 1021–1024.
- 23 M. Serantoni, A. S. Sarac and D. Sutton, *Surf. Coat. Technol.*, 2005, **194**, 36–41.
- 24 F. A. Stevie, L. A. Giannuzzi and B. I. Prenitzer, in *Introduction to Focused Ion Beams*, ed. L. Giannuzzi and F. Stevie, Springer, US, 2005, ch. 1, pp. 1–12.
- 25 A. Gaston, A. Z. Khokhar, L. Bilbao, V. Sáez-Martínez, A. Corres, I. Obieta and N. Gadegaard, *Microelectron. Eng.*, 2010, **87**, 1057–1061.
- 26 A. Al-Abboodi, J. Fu, P. M. Doran and P. P. Y. Chan, *Biotechnol. Bioeng.*, 2013, **110**, 318–326.
- 27 F. Boccafosci, M. Rasponi, C. Mosca, E. Bocchi and S. Vesentini, *Adv. Mater. Res.*, 2012, **409**, 105–110.
- 28 G. E. Murphy, K. Narayan, B. C. Lowekamp, L. M. Hartnell, J. A. Heymann, J. Fu and S. Subramaniam, *J. Struct. Biol.*, 2011, **176**, 268–278.
- 29 J. A. Heymann, D. Shi, S. Kim, D. Bliss, J. L. Milne and S. Subramaniam, *J. Struct. Biol.*, 2009, **166**, 1–7.
- 30 B. Liu, H. H. Yu, T. W. Ng, D. L. Paterson, T. Velkov, J. Li and J. Fu, *Microsc. Microanal.*, 2014, **20**, 537–547.
- 31 SRIM – The Stopping and Range of Ions in Matter, 2014, <http://www.srim.org>.
- 32 P. J. Cumpson, J. F. Portoles, A. J. Barlow, N. Sano and M. Birch, *Surf. Interface Anal.*, 2013, **45**, 1859–1868.
- 33 R. D. Kolasinski, J. E. Polk, D. Goebel and L. K. Johnson, *J. Vac. Sci. Technol., A*, 2007, **25**, 236.
- 34 FEI Company, Operation manual of dual beam system, 2014.
- 35 J. Muñoz-García, L. Vázquez, R. Cuerno, J. Sánchez-García, M. Castro and R. Gago, in *Toward Functional Nanomaterials*, ed. Z. M. Wang, Springer, US, 2009, ch. 10, vol. 5, pp. 323–398.
- 36 J. Fu, S. B. Joshi and J. M. Catchmark, *J. Micromech. Microeng.*, 2008, **18**, 095010.
- 37 J. Fu, S. B. Joshi and J. M. Catchmark, *J. Vac. Sci. Technol., A*, 2008, **26**, 422–429.
- 38 M. Guvendiren and J. A. Burdick, *Biomaterials*, 2010, **31**, 6511–6518.
- 39 M.-W. Moon, S. H. Lee, J.-Y. Sun, K. H. Oh, A. Vaziri and J. W. Hutchinson, *Proc. Natl. Acad. Sci. U. S. A.*, 2007, **104**, 1130–1133.
- 40 C. O. Yang, E. K. Her, K. H. Oh and T. J. Kang, *J. Korean Phys. Soc.*, 2012, **61**, 297–300.
- 41 J. Yin and C. Lu, *Soft Matter*, 2012, **8**, 6528.
- 42 B. Ziberi, F. Frost, B. Rauschenbach and T. Höche, *Appl. Phys. Lett.*, 2005, **87**, 033113.
- 43 D. E. Discher, P. Janmey and Y.-I. Wang, *Science*, 2005, **310**, 1139–1143.
- 44 C. E. Foerster, I. T. S. Garcia, F. C. Zawislak, F. C. Serbena, C. M. Lepienski, W. H. Schreiner and M. Abbate, *Thin Solid Films*, 2002, **411**, 256–261.
- 45 R. A. Frazier, M. C. Davies, G. Matthijs, C. J. Roberts, E. Schacht, S. J. B. Tendler and P. M. Williams, *Langmuir*, 1997, **13**, 4795–4798.
- 46 M. Radmacher, M. Fritz and P. K. Hansma, *Biophys. J.*, 1995, **69**, 264–270.

- 47 P. Krsko, S. Sukhishvili, M. Mansfield, R. Clancy and M. Libera, *Langmuir*, 2003, **19**, 5618–5625.
- 48 Y. Hong, P. Krsko and M. Libera, *Langmuir*, 2004, **20**, 11123–11126.
- 49 J. Jagielski, A. Turos, D. Bielinski, A. M. Abdul-Kader and A. Piatkowska, *Nucl. Instrum. Methods Phys. Res., Sect. B*, 2007, **261**, 690–693.
- 50 R. L. Clough, *Nucl. Instrum. Methods Phys. Res., Sect. B*, 2001, **185**, 8–33.
- 51 M. M. Hart and R. H. Adamson, *Proc. Natl. Acad. Sci. U. S. A.*, 1971, **68**, 1623–1626.
- 52 FEI Company, Material Safety Data Sheet Gallium.